Received: 19 December 2020 | Revised: 16 March 2021 | Accepted: 17 March 2021

DOI: 10.1002/er.6702

RESEARCH ARTICLE

INTERNATIONAL JOURNAL OF ENERGY RESEARCH WILEY

The examination of performance characteristics of a beta-type Stirling engine with a rhombic mechanism: The influence of various working fluids and displacer piston materials

Derviş Erol[1] | **Sinan Çalışkan**[2]

[1]Department of Automotive Technology, Kırıkkale Vocational School, Kırıkkale University, Kırıkkale, Turkey

[2]Department of Mechanical Engineering, Faculty of Engineering, Hitit University, Çorum, Turkey

Correspondence
Derviş Erol, Department of Automotive Technology, Kırıkkale Vocational School, Kırıkkale University, Kırıkkale 71450, Turkey.
Email: derol40@gmail.com

Summary

In this study, to develop a power generation system that can use renewable energy resources more efficiently, a beta-type Stirling engine with rhombic mechanism was designed and manufactured. Kinematic and thermodynamic analyses of a beta-type Stirling engine were performed numerically in the Fortran program. Volume and pressure changes depending on crankshaft angle of Stirling engine were made using the isothermal analysis. The effects of the basic parameters related to engine performance, such as working fluid mass, charge pressure, heater, and coolant temperatures, on the net work amount were investigated. Five different gases, including helium, air, nitrogen, carbon dioxide, and argon, were used as a working fluid in experimental studies. The effects of all these gases on engine performance characteristics were examined at charge pressures of 1 to 5 bar for two different displacer pistons made of stainless steel and titanium material. The performance characteristics of Stirling engine manufactured were tested using a specially designed electrical heater, at 727°C hot end and 27°C cold end temperature, depending on engine speed. In all experimental studies, maximum power output was acquired to be 215.48 W, at 4 bar and 550 rpm when a stainless steel displacer piston and helium gas as a working fluid were used, and maximum torque value was acquired to be 7.54 Nm, at 5 bar and 150 rpm. The lowest engine power output among maximum engine powers was acquired to be 34.66 W when argon gas was used as a working fluid at 3 bar and 300 rpm, using a displacer piston made of titanium material. Maximum power output acquired in the experimental studies using a stainless steel displacer piston and helium; it was determined that it is 72.12%, 73.69%, 241.49%, and 288.81% higher than the engine power acquired by nitrogen, air, carbon dioxide, and argon gases, respectively.

KEYWORDS

engine performance, kinematic analysis, rhombic mechanism, thermodynamic analysis, working fluids

Abbreviations: AISI, American Iron and Steel Institute; CFD, computational fluid dynamics; DAF, Van Doorne's Automobielfabrieken; DIN, Deutsches Institut für Normung; LPG, Liquid Petroleum Gas; MAN-MWM, Maschinenfabrik Augsburg-Nürnberg and Motoren Werke Mannheim; NASA, National Aeronautics and Space Administration; SAE, Society of Automotive Engineers.

1 | INTRODUCTION

The need for energy is predicted to increase in the coming decades.[1] A significant part of the increasing energy demand in areas, such as electricity, heating, and transportation, is met using nonrenewable sources of energy such as crude oil, coal, and natural gas.[2] The release of harmful emissions that are among the combustion products of fossil fuels into the atmosphere causes problems such as air pollution, ozone depletion, and global warming. The most common cause of greenhouse gas emissions worldwide is the use of fossil fuels. The excessive use of fossil fuels poses serious threats to the environment we live in and the future of the world.[3] The adverse effects, such as a decrease in the reserve resources of fossil fuels and an increase in energy costs, have become the most significant motivation behind the search for renewable energy sources that can replace fossil fuels. In recent years, one of the solutions to the concerns about energy is the use of renewable energy sources and increasing their usage areas.[4] Supplying the power needed by using renewable energy sources has become more common and important nowadays. It is observed that many developed countries are conducting studies so that 100% of their energy needs in areas such as electricity, heating, and transportation will be met by renewable energy sources until the 2050s.[5,6] Therefore, it is observed that the use and usage areas of renewable energy sources are increasing rapidly worldwide. Renewable energy sources nowadays can be listed as biomass energy, hydraulic (hydroelectric) energy, hydrogen energy, geothermal energy, ocean (wave and tidal) energy, solar energy, and wind energy. Solar energy represents the leading renewable energy source.[7]

Stirling engines were designed, invented, and manufactured by Robert Stirling, a Scottish clergyman, and engineer. In those years, Stirling engines were widely used in many different fields such as quarries and coal mines to meet the demand for energy due to their higher efficiency than steam engines.[8] With the invention of internal combustion engines in the 1860s, Stirling engines lost the superiority they gained compared to steam engines, and the interest in these engines decreased.[9] In 1937, studies on the development of Stirling engines and products were started in Philips Research Laboratories of the Netherlands to produce a little, silent, economical, and useful electric generator in order to meet the electricity needs of radios.[10] In the following years, large companies such as Cummins, DAF, Ford Motors, General Motors, MAN-MWM Group, NASA, Perkins, Siemens, and United Stirling conducted extensive investigation studies on Stirling technologies.[11] In the 1980s, since Stirling engines could not compete with internal combustion engines in terms of performance and energy efficiency, research and development studies carried out by large companies were terminated. It is observed that, since the day of their invention, Stirling engines have been used in a wide range of fields, such as agricultural irrigation, cooling machines, electricity generation, hydraulic pumps, marine vehicles, military systems, nuclear power stations, solar energy applications, water pumps, air conditioning systems and spacecraft, besides providing mechanical energy.[12]

Stirling engines are external combustion engines, and they can convert any kind of heat energy into mechanical energy. In Stirling engines, the heat energy from an external source is first transferred to working fluid, and then, this gas in the cylinder is expanded and converted into useful work. These engines can convert heat energy into mechanical energy by easily using different energy sources.[10] Stirling engines are divided into two groups, kinematic or free-piston engines. Kinematic Stirling engines are divided into three classes as alpha, beta, and gamma according to arrangement of moving parts, drive mechanisms, and cylinders. In alpha-type Stirling engines, the cycle is realized by working in harmony with each other by means of two separate cylinders, two separate power pistons, heater, cooler, and regenerator. A displacer piston is not used in these types of engines. The compression and expansion space are known as the spaces between the top points of both pistons in two separate cylinders. In beta-type Stirling engines, the cycle is realized by a piston and a displacer piston operating in the same cylinder. The displacer piston rod passes through the middle of the power piston. The compression space is located between power piston and displacer piston, and the expansion space is located in upper part of displacer piston. In gamma-type engines, cycle is realized by a power piston and a displacer piston operating in two separate cylinders.[11,12] Free-piston Stirling engines were first designed and patented by the professor William T. Beale at Ohio University. Free-piston Stirling engines consist of fewer parts compared to kinematic engines. In these engines, there is no mechanical connection between the displacer piston and the power piston.[13,14] They operate in line with the same principle of the thermodynamic cycle as kinematic Stirling engines. Free-piston Stirling engines have different applications such as electricity generation with a linear alternator, heat pump or cooling machine by moving the pistons back and forth in the cylinder. Furthermore, free-piston Stirling engines are preferred to meet the electrical needs of spacecraft by converting the heat energy of nuclear fuel into electrical energy in the dark regions of space where electricity cannot be generated from solar energy.[15,16] Stirling engines run with high efficiency, high performance, low fuel consumption, and without noise or vibration compared to internal combustion engines. Most of the heat losses occurring in Stirling engines are lost by cooling water. Due to the external combustion feature, harmful exhaust emissions such as hydrocarbon (HC), carbon monoxide (CO), and carbon dioxide (CO_2) are much less and controlled compared to internal combustion engines.[17,18] Various power generation methods and machines are developed to meet energy demands using renewable energy sources. Stirling engines, one of these alternative power generating machines, can easily use many renewable energy sources due to their external combustion feature and have again taken their place at the top of the energy generation required due to positive developments in production technology compared to other power generation systems. Therefore, research and development studies on low-emission, high-efficiency, and high-performance Stirling engines that can generate power using cheaper and easily available renewable energy sources have gained momentum again nowadays.[19]

There are many theoretical and experimental studies on Stirling engines with rhombic mechanisms in the literature. Eid conducted theoretical research by performing the analysis that was developed by Gustav Schmidt on a beta-type Stirling engine. In that study, power-displacer stroke, regenerator, cooler, and heater were accepted as non-dimensional, and the optimum working conditions were determined. Furthermore, the effects on performance characteristics of Stirling engine were investigated by placing stainless square wire cages as regenerative medium on the displacer piston used in the study and it was stated to provide approximately 20% more engine power increase.[20] Shendage et al conducted theoretical research on slider-crank and rhombic mechanisms in a Stirling engine without changing their characteristics, operating parameters, and geometry. They reported that the Stirling engine with rhombic mechanism produced 10% more power than slider-crank mechanism.[21] Solmaz and Karabulut investigated performance characteristics of a beta-type Stirling engine with bell-crank and rhombic mechanisms.[22] In their study, Aksoy et al theoretically examined the effects of slider-crank and rhombic mechanisms in a beta-type Stirling engine on engine performance.[23] Salazar and Chen theoretically examined the heat transfer characteristics of a beta-type Stirling engine using the computational fluid dynamics (CFD) analysis program.[24] In 2015, Chen et al theoretically investigated the effects of gas movements in regenerator on engine performance using the CFD analysis program.[25] Zainudin et al theoretically examined the thermodynamic analysis of a rhombic mechanism. In that research, the thermodynamic assessments of a Stirling engine using a numerical model were made by the isothermal analysis. It was predicted that 805 W engine output and 50.1% efficiency could be acquired at 300 rpm from the engine for which theoretical analysis was performed.[26] Many theoretical and experimental studies on Stirling engines with a rhombic mechanism have been carried out by Xiao et al from 2014 to the present day.[27-29] In 2016, the effects of helium and nitrogen working fluids on engine performance were studied theoretically and experimentally with a new parametric analysis approach in a Stirling engine with rhombic mechanism.[30] Furthermore, in another study, engine performance parameters such as temperature, velocity vectors, and pressure-volume changes in compression-expansion areas were compared using the CFD analysis program.[31] Wang et al developed a third-order numerical model based on a one-dimensional computational fluid dynamics model for kinematic Stirling engines. The effects of helium and hydrogen working fluids on engine performance were compared theoretically and experimentally. The researchers stated that the Stirling engine, which used helium as the working fluid, had much lower optimum operating frequencies and lower engine performances compared to the engine using hydrogen and showed both experimental and theoretical results.[32] Abuelyamen et al carried out a numerical study on a beta-type Stirling engine with a rhombic mechanism using the ANSYS fluent 14.5 analysis program. In that study, basic information on engine performance, such as P-V diagrams, heat transfer occurring in the engine, heater, and coolant temperature, was determined theoretically and graphically in comparison with air, helium, and hydrogen working fluids.[33] Alfarawi conducted theoretical performance and thermodynamic analyses for slider-crank and rhombic mechanisms under the same conditions for a beta-type Stirling engine. In that study, thermodynamic calculations using a numerical model were made. It is reported that the rhombic mechanism generates 32% more power and provides 20% more efficiency than slider-crank mechanism in the same conditions.[34] Solmaz et al theoretically examined using the response surface method the effects on performance characteristics of a beta-type engine with rhombic mechanisms. As a result of the theoretical studies, the predicted performance values were compared with the performance results obtained in experimental studies. According to the results, researchers were reported that amounts of engine power output and torque were 868.13 W and 11.95 Nm, respectively, under optimal engine working conditions. Furthermore, specific power output was found to be 1100 W/L which was 13% higher than previous study.[35]

Cheng et al have conducted many theoretical and experimental studies on beta-type Stirling engines with rhombic mechanism since 2010. According to the power values of these developed engines, it is observed with each new study that performance characteristics were improved from 0.3 to 1.3 kW.[36-42] Recently, Cheng et al developed a prototype beta-type Stirling heat pump for hot water supply and performed performance tests. In that study, a thermodynamic model was developed to predict performance of the Stirling heat pump, and theoretical analyses were conducted. The experimental results of a 1 kW-class prototype Stirling heat pump were compared to check the accuracy of the theoretical results obtained. It was stated that the experimental studies were performed with helium gas at 5 bar and a constant engine speed of 1000 rpm. According to the results, it was reported that hot water could be produced with a heating power of 904 W and at a temperature of 38°C under a water flow of 1 (L/min).[43] In another study conducted by the researchers, they performed theoretical analyses to predict heat transfer and engine performance characteristics with the help of a CFD analysis program in a beta-type Stirling engine. As a result of the theoretical studies, the predicted performance values were compared with the performance results obtained in experimental studies. In the experimental studies, it was reported that maximum power was acquired to be 507.3 W with helium gas at 15 bar.[44] Li et al produced a Stirling engine with rhombic mechanism using waste gases and carried out its experimental studies. As a result of the tests, it was stated that maximum power output of 3476 W was acquired at an engine speed of 1248 rpm. It was explained that maximum power value acquired was very close to the results of the theoretical analysis.[45] Duan et al performed the design, optimization, manufacturing, and performance tests of a beta-type Stirling engine with a rhombic mechanism. Furthermore, in the study, a heat exchanger was developed to decrease gas flow losses in the cylinder. It was indicated that an electric heater system and air as the working fluid were used in experimental studies. As a result of the tests, it was reported that a maximum power output of 288 W was achieved at 15 bar and a heater temperature of 600°C. Furthermore, it was stated that improving the sealing problems of the Stirling engine and reducing clearance volumes in heat exchangers would lead to better engine performance results.[46]

Çınar et al conducted a study involving the design, manufacture, and performance tests of a Stirling engine with a rhombic mechanism.[47] The performance tests of the Stirling engine were carried out using a liquid petroleum gas (LPG) fueled heater, air and helium gases at different operating pressures. It was stated that maximum power output was 95.77 W at 575 rpm with heater temperature of 450°C, 2 bar, and helium as working fluid, and maximum torque was acquired to be 1.98 Nm at 410 rpm.[48] In 2015, a beta-type Stirling engine with a rhombic mechanism was designed and manufactured as a master's thesis study at Afyon Kocatepe University. The performance tests of this engine were conducted at different charge pressures with an LPG fueled heater as a heat source under laboratory conditions. The maximum power was reported to be 244 W at a heater temperature of 700°C, 3 bar, and 466 rpm engine speed.[49] In a new study conducted in 2016, modifications were made to the same engine, which became with a regenerator. In the experimental studies, maximum power output was acquired to be 2353 W at 5 bar and 1099 rpm using a regenerator. It was stated that a 28.53% increase was acquired in engine power with the use of regenerators.[50,51] Çınar et al designed and produced two different rhombic mechanisms in equal situations for a Stirling engine having the same cylinder, power piston, and displacer piston dimensions and equal swept volume. In one of these mechanisms, two spur gears were used, and gear shaft was supported in bearings from one side covers. In other mechanism, two helical gears were located on crankshafts that supported with bearings on both side covers. In the experimental studies using helical gears, maximum power output was acquired to be 663 W at 4 bar. The researchers declared that engine output increased by 132%, while frictional damages and gear sounds were decreased by supporting mechanism from both sides and using helical gears.[52]

There are many studies in the literature which use air and helium gases as the working fluid in Stirling engines. There are only a few experimental and theoretical studies using nitrogen gas as the working fluid in Stirling engines. In addition, the lack of studies that use carbon dioxide and argon gas is considered to be a major deficiency. In this context, when the studies in the literature are examined, there is no study that examines the effects of both five different working fluids and the type of displacer piston material on engine performance experimentally. Therefore, such study was conducted due to the motivation of this study contributing to the literature. In the present study, it was planned to develop a power generation system that could use renewable energy resources more efficiently. In this context, a beta-type Stirling engine with rhombic mechanism and a swept volume of 365 cm^3 was designed, manufactured, and tested. The performance characteristics of this engine were studied numerically and experimentally for different operating parameters. Five different gases, including helium, air, nitrogen, carbon dioxide, and argon, were used as a working fluid in experimental studies. Also, the effects of all these gases on engine performance characteristics were examined at charge pressures of 1 to 5 bar for two different displacer pistons made of stainless steel and titanium material. Better performance characteristics were acquired in the experimental studies using a stainless steel displacer piston and helium gas.

2 | KINEMATICAL AND THERMODYNAMIC ANALYSES OF RHOMBIC MECHANISM

The rhombic mechanism was first used in Stirling engines in 1953 by Dr. Roelof Jan Meijer, working as an engineer at the Philips Company.[53] As seen in the scheme in Figure 1, the rhombic mechanism consists of the connecting rods with six sides equal to each other, two synchronized gears, and a crankshaft rotating in a balanced way in opposite directions. Power piston rod is connected to the upper connecting part, while the displacer rod is connected to the lower connecting part. The most significant advantage of this mechanism is that the lateral friction forces between the power and displacer piston rods are very low. Since the lateral friction forces are low, it reduces the wear that may occur on the parts and provides an increase in power and torque. The technical characteristics of Stirling engine with rhombic mechanism, for which thermodynamic and kinematic analyses have been conducted, are presented in Table 1.

2.1 | Kinematical analysis

Kinematic investigates the movements of objects without considering masses and forces that are effective on them. The parameters such as cyclic work, pressure, and volume of an existing system and the performance properties may be determined with the thermodynamic analysis method before prototypes are made. The kinematic analysis and operating parameters of Stirling engine, the scheme of which is presented in Figure 1, were entered in the Fortran program using Equations (1) to (9) and examined numerically.[21,38,47,54]

TABLE 1 Technical properties of prototype Stirling engine with a rhombic mechanism

Engine type	Beta
Swept volume (cm^3)	365
Displacer cylinder bore, Dd (mm)	88
Displacer piston bore (mm)	87
Displacer piston length, hd (mm)	200
Displacer piston stroke (mm)	60
Power cylinder bore, Dp (mm)	88
Power piston bore (mm)	87.97
Power piston length, hp (mm)	130
Power piston stroke (mm)	60
Cylinder length, Ht (mm)	517
Distance between gear axes, L (mm)	132.5
Displacer rod length, ldr (mm)	340
Displacer rod bore, Dr (mm)	16
Connecting rod length, lr (mm)	66.23
Crank Radius, Rc (mm)	24.838

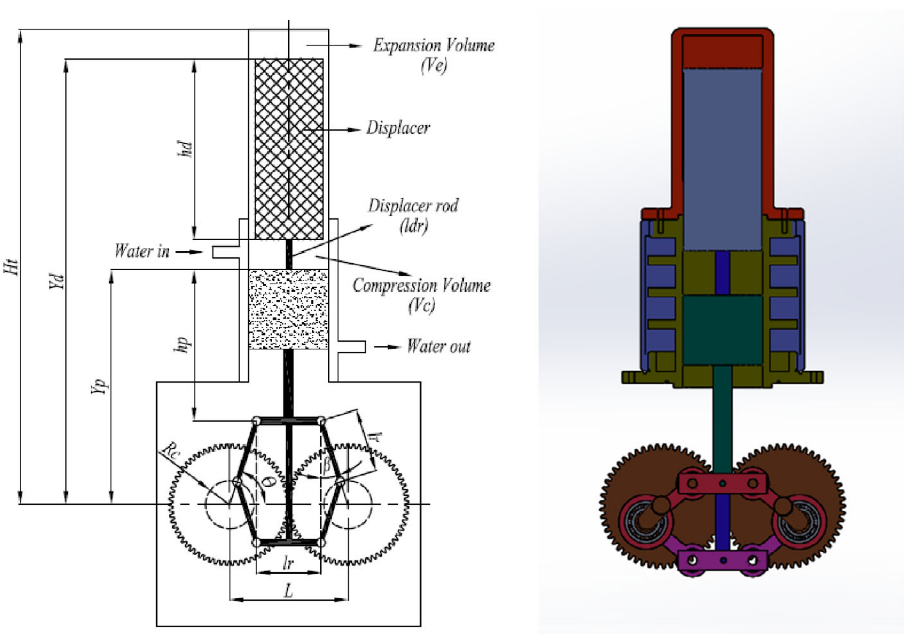

FIGURE 1 Schematic views of the prototype Stirling engine with a rhombic mechanism [Colour figure can be viewed at wileyonlinelibrary.com]

The distance from top point of power piston to the axis of the crank,

$$Y_p = \left[lr^2 - \left(\left(\frac{L - lr}{2} \right) - (R_c \text{Cos}\theta) \right)^2 \right]^{1/2} + (R_c \text{Sin}\theta) + (h_p) \quad (1)$$

The distance from top point of displacer piston to the axis of the crank,

$$Y_d = (l_{dr} + h_d) - \left[lr^2 - \left(\left(\frac{L - lr}{2} \right) - (R_c \text{Cos}\theta) \right)^2 \right]^{1/2} + (R_c \text{Sin}\theta) \quad (2)$$

The length of the cold volume,

$$e_c = Y_d - h_d - Y_p \quad (3)$$

The variation of the cold volume,

$$V_c = e_c (A_p - A_{dr}) \quad (4)$$

The area of the power piston,

$$A_p = \left(\frac{\pi D_p^2}{4} \right) \quad (5)$$

The area of the displacer rod,

$$A_{dr} = \left(\frac{\pi D_r^2}{4} \right) \quad (6)$$

The length of the hot volume,

$$e_e = H_t - Y_d \quad (7)$$

The variation of the hot volume,

$$V_e = e_e A_d \quad (8)$$

The area of the displacer piston,

$$A_d = \left(\frac{\pi D_d^2}{4} \right) \quad (9)$$

The compression, expansion, and total volume changes of the Stirling engine depending on crankshaft angle, acquired using the Fortran program are given in Figure 2. When Figure 2 is examined, although the power piston and displacer piston have the same stroke, the compression volume and expansion volume values are different from each other, which is caused by the fact that the power piston moves in the direction to the bottom dead center while the displacer piston continues to move in direction to the top dead center. Therefore, the compression volume is different from the swept volume. The expansion volume and swept volume values are approximately equal to each other. Furthermore, compression volume value remains constant specific to this mechanism for a period of approximately 90° after the 180° position of the crankshaft. In other words, the compression process is performed at a constant temperature for a period of 90°.

The power piston and displacer piston position values acquired using the Fortran program depending on crankshaft angle of the Stirling engine with a rhombic mechanism are given in Figure 3. When the graph is examined, it is observed that the stroke lengths of the power and displacer pistons are 60 mm. As can be seen from the graph, the power and displacer pistons move in unison towards the top dead center for a period of approximately 90° starting from the 180 ° position of the crankshaft, which indicates that there is no contact between the pistons.

2.2 | Thermodynamic analysis

Using the isothermal analysis method developed by Professor Gustav Schmidt from the German Polytechnic Institute in 1871, the performance parameters of an existing system like pressure, volume, and power may be

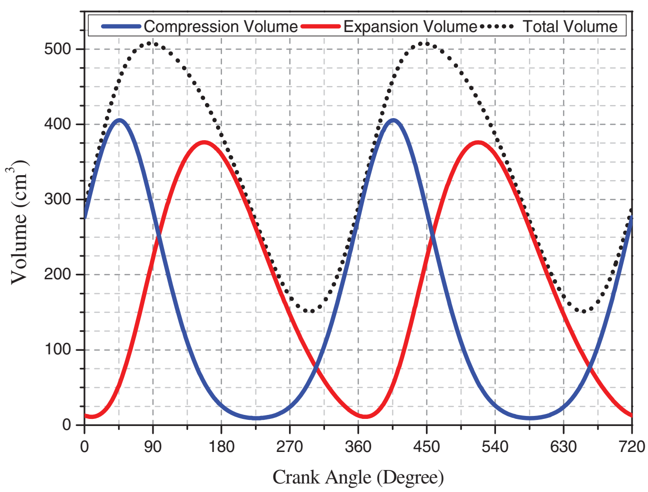

FIGURE 2 The variation of volume according to the different crank angle of the rhombic mechanism [Colour figure can be viewed at wileyonlinelibrary.com]

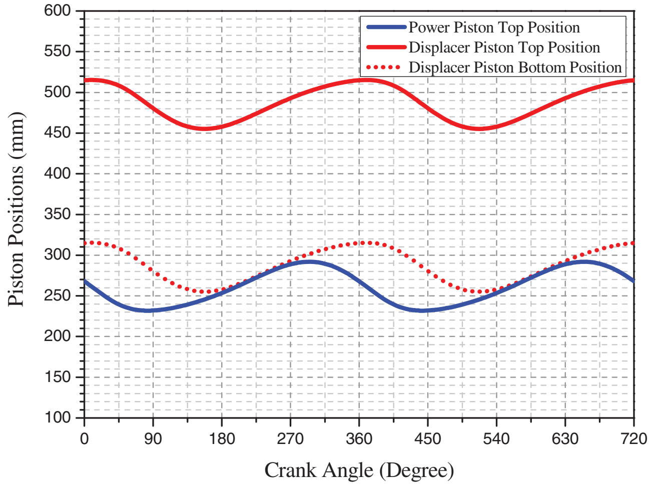

FIGURE 3 The variation of piston positions according to the different crank angle of rhombic mechanism [Colour figure can be viewed at wileyonlinelibrary.com]

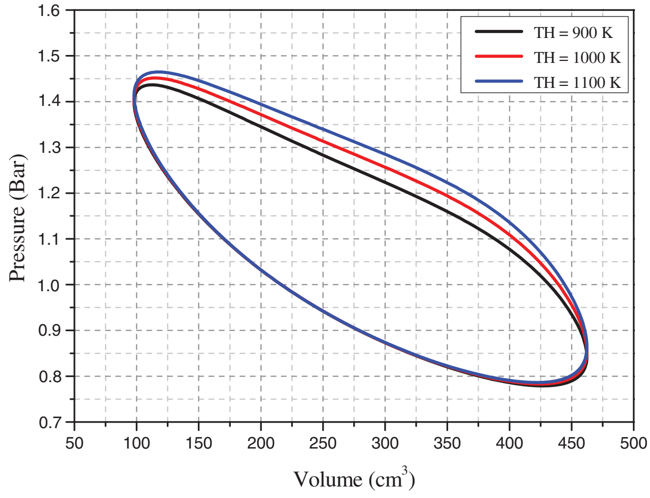

FIGURE 4 Comparison of P-V diagrams for different heater temperatures of the rhombic mechanism [Colour figure can be viewed at wileyonlinelibrary.com]

determined theoretically before engine prototypes are produced. In this analysis method, all of the heat losses in the Stirling engine are neglected. In isothermal analysis, it is considered that whole heat input to system occurs in the expansion space, while the heat output released from the system occurs in the compression space at a constant temperature. Therefore, in the analysis, temperatures of the gas masses in the expansion space, compression space, and regenerator are taken as equal to the internal wall temperatures. This basic assumption of the analysis allows for developing a simple mathematical equation for working fluid pressure as a function of volume variations. The equations used in determining changes in the net work and pressure acquired from Stirling engines are given in Equations (10) and (11). Due to the assumptions that compression and expansion processes occur isothermally and there are no aerodynamic gas flow losses, the isothermal analysis developed by Schmidt provides mathematical solution convenience rather than fully expressing the system performance. The following assumptions were made while employing the isothermal analysis method.[54,55]

- Working gases are considered a perfect gas.
- The working gas mass is constant throughout the cycle, and there are no leaks.
- The kinetic and potential energies of the working gas are neglected.
- The engine cyclic is established in a steady state.
- The speed of the engine is constant.
- During the volume change in the compression and expansion spaces, the temperature of the working gas is equal to T_H and T_L temperatures.

Pressure in isothermal analysis,

$$P = m.R\left(\frac{V_1}{T_1} + \frac{V_2}{T_2} + \ldots.. + \frac{V_n}{T_n}\right)^{-1} \tag{10}$$

Net work,

$$W = \sum_{i=1}^{i=k} P_i(V_i - V_{i-1}) \tag{11}$$

equations are used.

The comparison of P-V diagrams depending on different heater temperatures of Stirling engine with rhombic mechanism is given in Figure 4. During thermodynamic analyses the mass of the working fluid was kept constant at 0.000536 kg and the coolant temperature was kept constant at 300 K. The cyclic work values of this engine with a rhombic mechanism were calculated as 10.66, 11.61, and 12.42 J, for different heater temperature, respectively. The net work output is thus acquired from Equation (11).

The variations of pressure-volume for the compression, expansion, and total spaces of the Stirling engine are given in Figure 5. In the thermodynamic analysis for 1000 K heater temperature, 300 K cooler temperature, and 0.000536 kg fixed working fluid, the net work amount obtained from the engine with rhombic mechanism during one cycle was obtained to be 11.61 J. The compression, expansion, and total spaces cycled under these conditions are separately presented in the graph.

The comparison of P-V diagrams at different charge pressures, depending on volume change of Stirling engine with a rhombic mechanism, is given in Figure 6. The mass of the working fluid varies at a certain rate as the amount of charge pressure increases. The coolant and heater temperatures were kept constant at 1000 and 300 K, respectively, during a cycle for 1 to 5 bar charge pressures. Under these conditions, the cyclic work values of this engine with a rhombic mechanism were acquired as 11.61, 23.22, 34.83, 46.44, and 58.05 J, respectively. When the graph and results are examined, it is determined that the net cyclic work amount performed increases in direct proportion to the charge pressure.

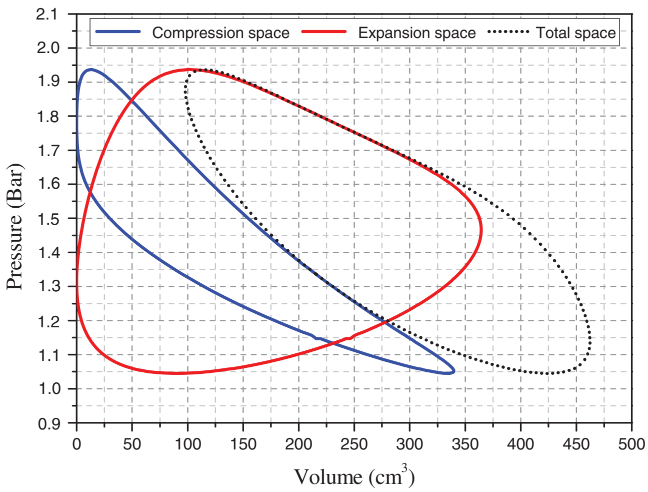

FIGURE 5 The variation of P-V diagrams for the compression, expansion, and total spaces [Colour figure can be viewed at wileyonlinelibrary.com]

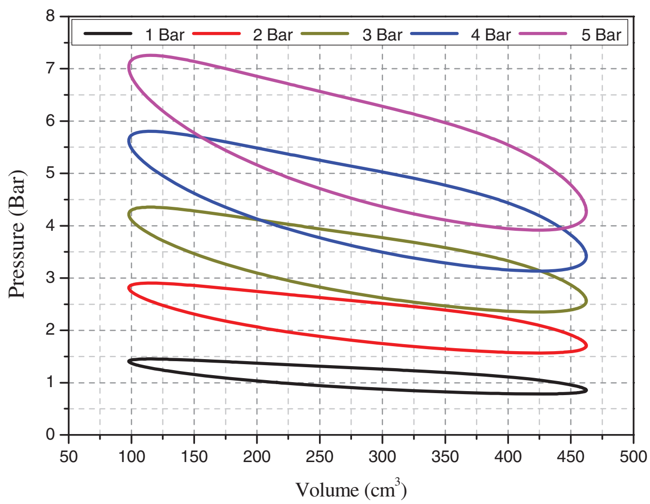

FIGURE 6 Comparison of P-V diagrams for different pressures of rhombic mechanism [Colour figure can be viewed at wileyonlinelibrary.com]

3 | MATERIAL AND METHOD

The design and manufacturing drawings of the beta-type Stirling engine with a rhombic mechanism were performed using SolidWorks which is computer-aided design program. The explanations and schematic images belonging to material features of basic engine parts such as engine block and side covers, crankshaft, rhombic gears, power cylinder, power piston, displacer cylinder and piston, displacer piston rod, connecting rods, and engine flywheel are presented below. The assembly view of the manufactured rhombic mechanism can be observed in Figure 7.

The engine block was manufactured out of spheroidal cast iron material in one piece to withstand the 10 bar of the working fluid. The two sides of the engine block are closed by two covers, which also serve as bed-plate for the crankshaft. The side covers were made out of AISI/SAE 1040 (DIN C40 Carbon Steels) material. The outer rings of the tapered bearings in the main trunnions of the crankshaft were located on the centering niches on the

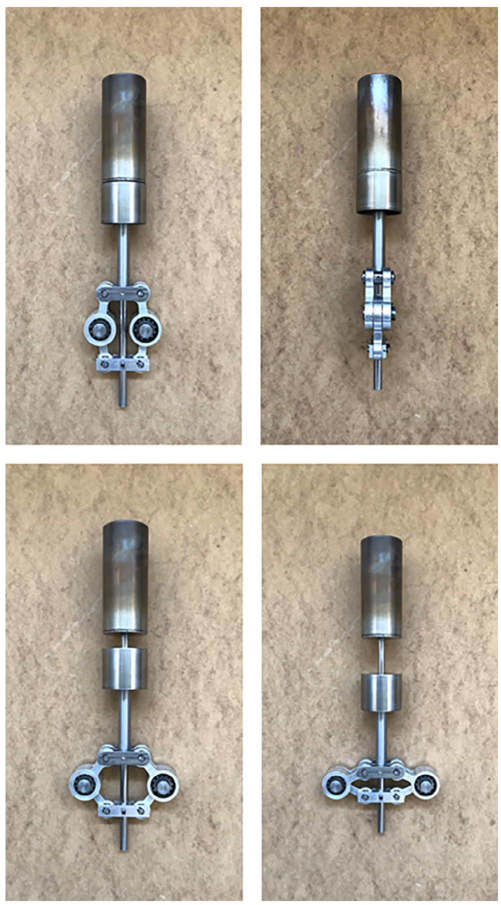

FIGURE 7 Assembly view with a rhombic mechanism of the power and displacer pistons [Colour figure can be viewed at wileyonlinelibrary.com]

covers of the block. The covers fix the crankshaft on both sides by means of tapered bearings. Sealing channels were engraved for the use of a special sealing gasket on the side cover surfaces and engine block to ensure the sealing of the Stirling engine. Since its surface hardening and toughness feature is high, the crankshaft was manufactured out of AISI/SAE 4140 (DIN 42CrMo4) material in one piece. The trunnion surfaces were sensitively ground, and after the crankshaft trunnions were ground, the surface quality was improved by polishing. After these operations, the trunnion surface of the crankshaft was heat treated to increase its resistance to abrasion, torsion, and bending stresses. Two different helical gears rotating in opposite directions were used to the right and left of the rhombic mechanism. Gears were manufactured out of AISI/SAE 4140 material in one piece. Rhombic gears were connected to the crankshaft with bolts.

The power cylinder was manufactured using AISI/SAE 1040 material in one piece. A pre-set working clearance is essential between the cylinder and the power piston, to allow for comfortable operation. The inner surface where the power piston would work was honed in a way to give a working clearance of 0.03 mm. Stepped fins were mounted on the outer side of the power cylinder to facilitate easier cooling of working fluid. The outer part of power cylinder was sealed with the help of the cooling jacket manufactured in one piece out of aluminum 7075 material (AlZn5.5MgCu).

The power piston was manufactured out of spheroidal graphite cast iron material due to its high lubrication and abrasion resistance and the low amount of expansion due to high temperature. Since the rod of the displacer piston passes through the middle of power piston in beta-type engines, bronze material is placed in the middle of the power piston and rod and turned and processed precisely. Thus, mechanical losses were minimized by providing better quality sealing between power piston rod and displacer piston rod.

In this study, two different displacer pistons were manufactured out of AISI/SAE 303 (DIN X8CrNiS18-9 stainless steel) and Ti 6Al 4 V (GR5 titanium) materials, and their effects on engine performance were investigated experimentally. One of the displacer pistons was manufactured out of AISI/SAE 303 (DIN X8CrNiS18-9) material in the hollow form due to its easy processability, corrosion resistance, and high mechanical properties. Stainless steel covers were welded into both open ends of the displacer piston so that no working fluid could get inside. The bottom end of the displacer piston was specifically threaded to facilitate the connection of the displacer rod. The displacer cylinder was manufactured out of AISI/SAE 303 tube material in one piece due to its easy processability, corrosion resistance, and high mechanical properties. The other second displacer piston was manufactured out of titanium (Ti-6Al-4 V/GR5) material in the hollow form due to its easy processability, very lower thermal conductivity, low density, excellent corrosion resistance, superb strength-weight ratio, and superlative thermal stability.[56,57] In addition to these superior features, the cost of a titanium displacer piston is considerably higher than a stainless steel displacer piston.

Connecting rods were manufactured out of aluminum 7075 material in one piece due to its light weight and easy processability, corrosion resistance and high mechanical properties. As is seen in Figures 7 and 8, in the rhombic mechanism manufactured, four connecting rods were used for the power piston, and two connecting rods were used for the displacer piston. When Figure 9 is examined, special bearings were mounted on the connecting rods to minimize wear and noise values that might occur under the operating conditions of the engine.

4 | RESULTS AND DISCUSSION

The experimental studies were carried out in the laboratory of Kırıkkale University Automotive Technology Department. Five different gases, including helium, nitrogen, air, carbon dioxide, and argon were used as a working fluid in experimental studies. The effects of all these working fluids on engine performance characteristics were examined at different engine charge pressures (1 to 5 bar) for two different displacer pistons made of stainless steel and titanium material. The performance characteristics of the manufactured Stirling engine were tested using a specially designed electrical heater, at 727°C (±10°C) hot end and 27°C (±5°C) cold end temperature, depending on engine speed. The experimental setup and auxiliary equipment of the Stirling engine are given in Figure 10.

The study maps of engine power characteristics obtained in the experimental studies conducted with different working fluids in stainless steel and titanium displacer pistons depending on engine speed and charge pressure are presented in Figure 11. In Stirling engines, working fluid passes bidirectionally between hot and cold regions, through space between regenerator or displacer piston and cylinder wall. After the working fluid converts the heat energy received from the hot source into mechanical energy, the cycle is completed by transferring the remaining heat energy to the cold source. This process is repeated during each cycle. Along with the increase in engine speed, the heating-cooling times

FIGURE 8 General views of prototype engine parts manufactured [Colour figure can be viewed at wileyonlinelibrary.com]

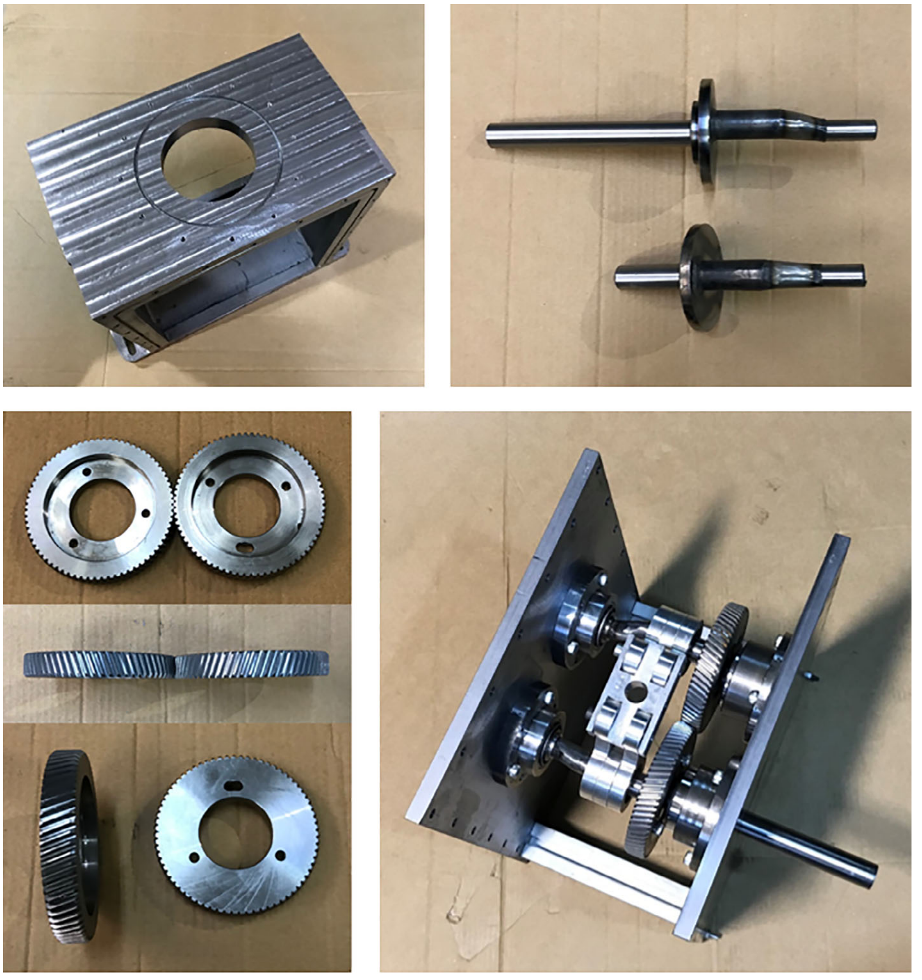

FIGURE 9 Connecting rods [Colour figure can be viewed at wileyonlinelibrary.com]

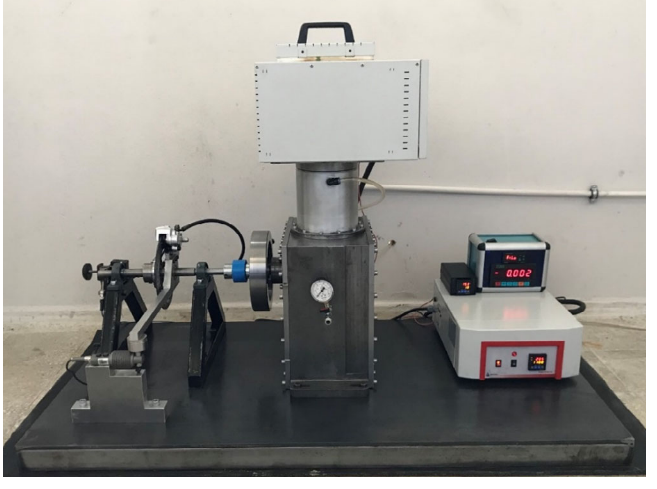

FIGURE 10 View of the experimental setup of Stirling engine and measuring devices [Colour figure can be viewed at wileyonlinelibrary.com]

applied to the working fluid throughout the cycle are proportionally reduced. Therefore, the working fluid used in Stirling engines is desired to have a high thermal conductivity. When the performance maps in Figure 11 are examined, it is observed that the displacer piston material used did not have a significant effect on the performance values of Stirling engines. However, it was observed that the thermal conductivity and density of the working fluid had a significant effect on the performance values of Stirling engines.

The change in the engine performance characteristics, depending on engine speed, acquired in the experimental studies conducted with stainless steel and titanium

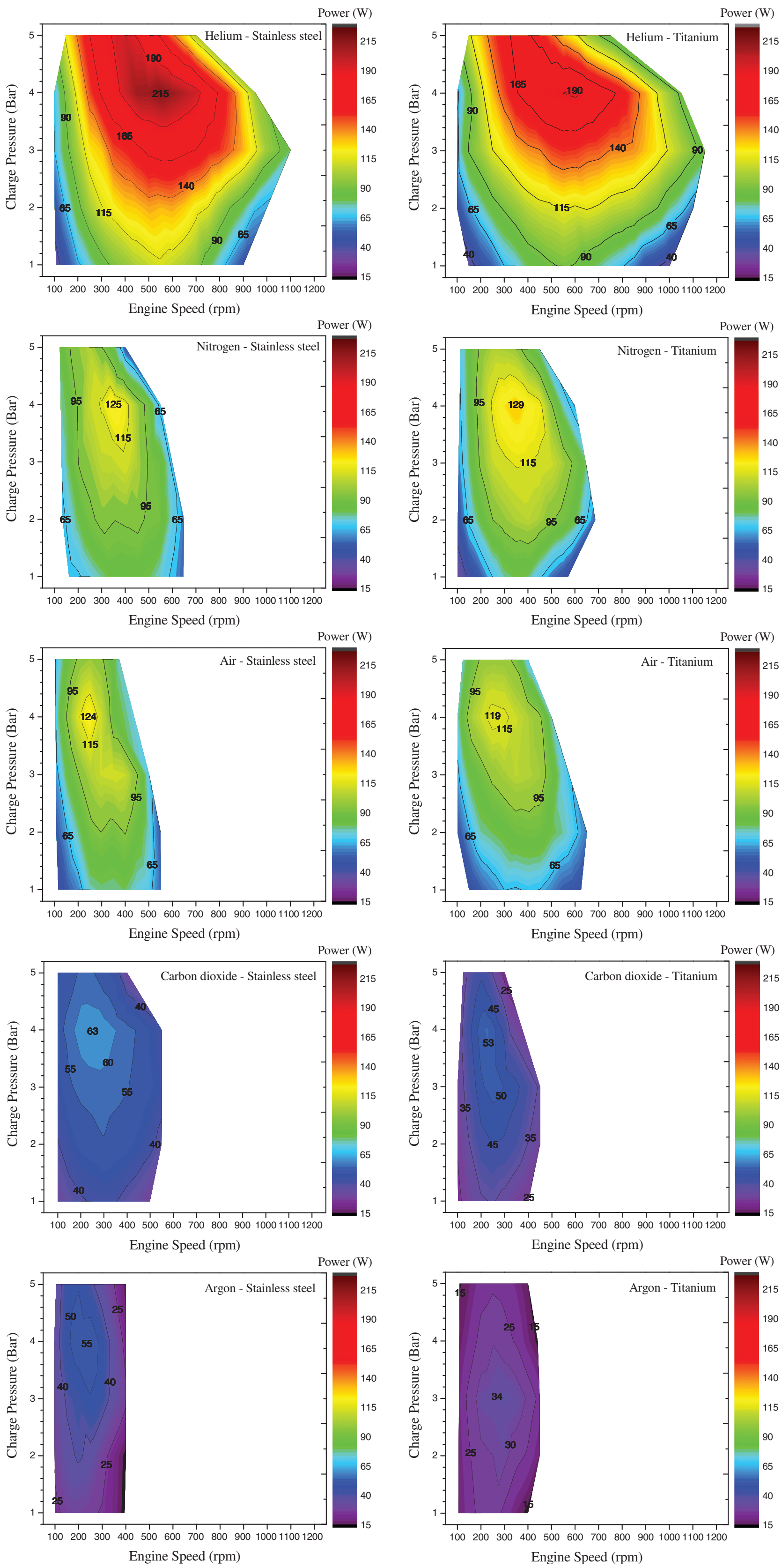

FIGURE 11 View of engine performance maps; helium, nitrogen, air, carbon dioxide, and argon respectively [Colour figure can be viewed at wileyonlinelibrary.com]

displacer pistons and helium as working fluid at different engine charge pressures, is given in Figure 12. As seen in Figure 12A, the maximum power values in the experiments conducted with a stainless steel displacer piston were acquired to be 112.78, 134.07, 172.34, 215.48, and 195.93 W, respectively, for pressures of 1, 2, 3, 4, and

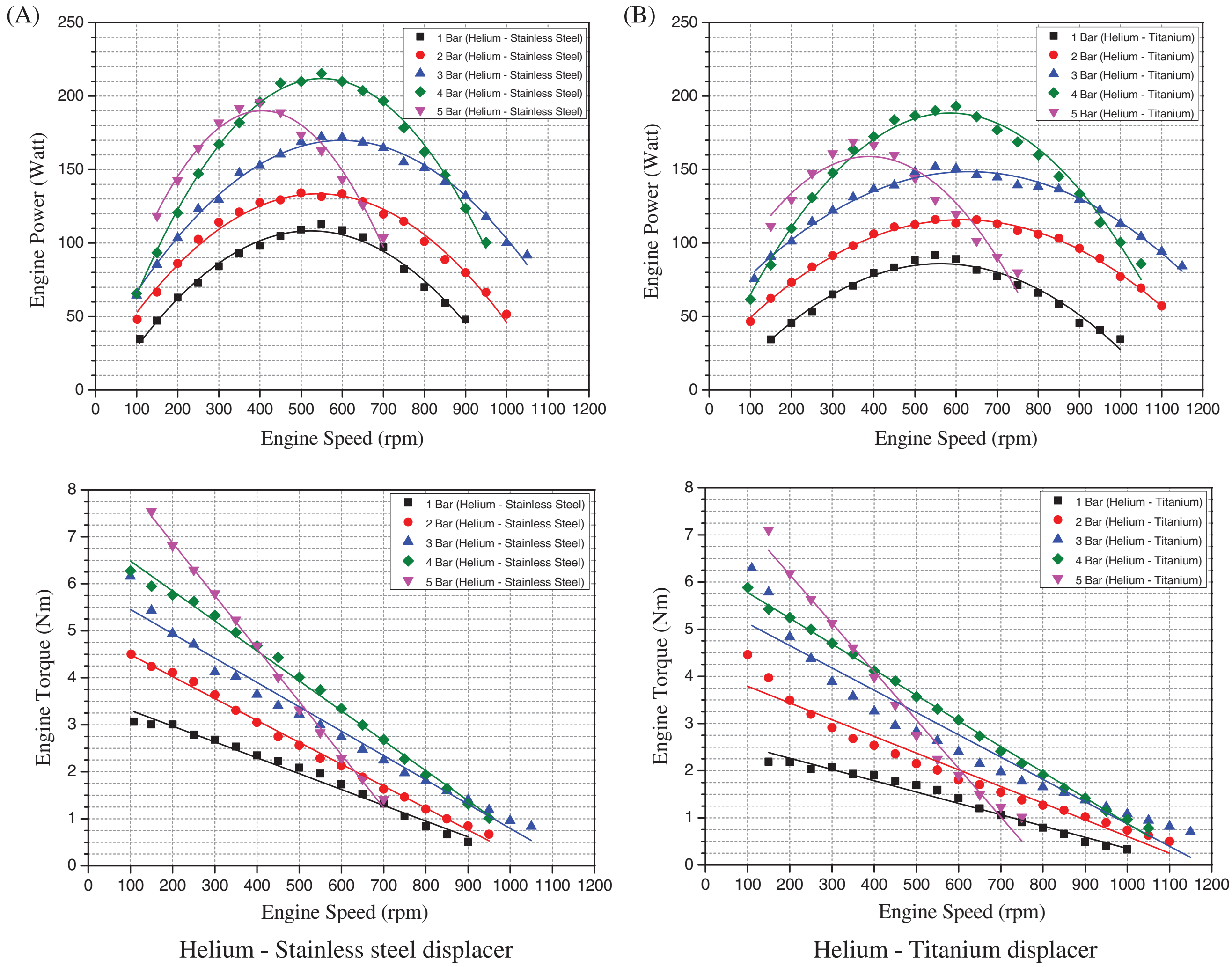

FIGURE 12 The variations of engine power and torque depending on engine speeds at different charge pressures [Colour figure can be viewed at wileyonlinelibrary.com]

5 bar. Maximum torque values were measured to be 3.07, 4.49, 6.16, 6.27, and 7.54 Nm, respectively. In the case of using helium gas, maximum power output was acquired to be 215.48 W, at 4 bar and 550 rpm, and maximum torque value was acquired to be 7.54 Nm, at 5 bar, and 150 rpm. This engine power acquired is the highest value acquired under all experimental conditions with stainless steel and titanium displacer pistons and nitrogen, air, carbon dioxide, and argon as working fluid. Thermal conductivity of working fluids has a very significant effect on engine performance characteristics. While the thermal conductivity of helium gas at 1000 K is 0.4052 W/mK, the thermal conductivity of air, carbon dioxide, nitrogen, and argon gases at the same temperature is 0.06754, 0.06752, 0.0626, and 0.0493 W/mK, respectively. As can be seen from these values, the thermal conductivity of helium gas is much higher compared to other gases. Furthermore, helium gas has less friction loss due to its density and viscosity compared to other gases.

As seen in Figure 12B, the maximum engine power values in the experiments conducted with a titanium displacer piston were acquired to be 91.68, 116.07, 151.94, 193.12, and 168.91 W, respectively, for pressures of 1 to 5 bar. Maximum torque values were measured to be 2.19, 4.46, 6.28, 5.88, and 7.1 Nm, respectively. Maximum power output was acquired to be 193.12 W, at 4 bar and 600 rpm, and maximum torque value was acquired to be 7.1 Nm, at 5 bar and 150 rpm. This engine power acquired is the highest value acquired under all experimental conditions with a titanium displacer piston and nitrogen, air, carbon dioxide, and argon as working fluids. Furthermore, it was determined that maximum power output value acquired at 4 bar in the titanium displacer piston was 10.38% less in comparison with the stainless steel displacer piston.

The change in the engine performance characteristics, depending on engine speed, acquired in the experimental studies conducted with stainless steel and titanium displacer pistons and nitrogen as working fluid at different engine charge pressures, is given in Figure 13. As seen in Figure 13A, the maximum power values in the experiments conducted with a stainless steel displacer piston were acquired to be 82.81, 99.24, 112.77, 125.19, and 105.1 W, respectively, for pressures of 1 to 5 bar. Maximum torque values were measured to be 3.56, 4.3, 4.93, 5.07, and 6.19 Nm, respectively. In the case of using nitrogen gas, maximum power output was acquired to be 125.19 W, at 4 bar and 350 rpm, and maximum torque value was acquired to be 6.19 Nm, at 5 bar and 150 rpm. While the thermal conductivity of nitrogen gas at 1000 K is 0.0626 W/mK, the thermal conductivity of air and carbon dioxide gases at the same temperature is 0.06754 and 0.06752 W/mK, respectively. As can be seen from these values, the thermal conductivities of nitrogen, air, and carbon dioxide gases are very close to each other. The maximum power values acquired from the experiments conducted on using a stainless steel displacer piston and nitrogen, air, and carbon dioxide gases as working fluids are 125.19, 124.06, and 63.1 W, respectively. Furthermore, it was determined that maximum power output value acquired by using nitrogen gas as working fluid at 4 bar produced 0.91% and 50.4% more power, respectively, than that acquired by using air and carbon dioxide gases. Although the thermal conductivity of these gases is close to each other, the engine powers acquired are different from each other. The acquired engine powers show that the viscosity and density of the gases used as working fluid have significant importance for engine performance. While the density of nitrogen gas at 1000 K temperature is 0.318 kg/m^3, the densities of air and carbon dioxide gases at the same temperature are 0.353 and 0.536 kg/m^3, respectively. Since the density of carbon

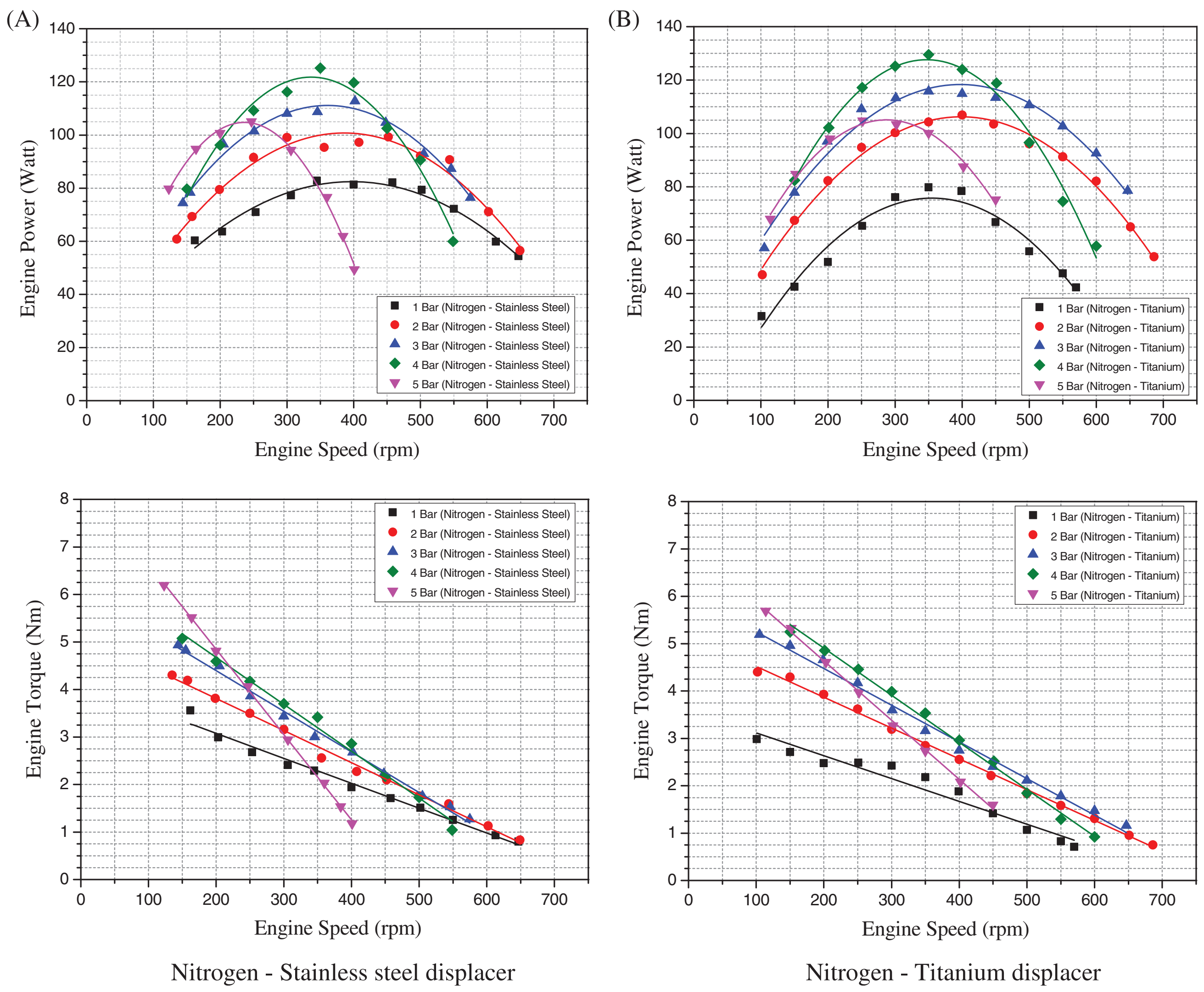

FIGURE 13 The variations of engine power and torque depending on engine speeds at different charge pressures [Colour figure can be viewed at wileyonlinelibrary.com]

dioxide gas is higher than other gases, it affects engine performance adversely.

As seen in Figure 13B, the maximum engine power values in the experiments conducted with a titanium displacer piston were acquired to be 79.83, 106.92, 115.79, 129.52, and 104.75 W, respectively, for pressures of 1 to 5 bar. Maximum torque values were measured to be 2.98, 4.4, 5.19, 5.25, and 5.69 Nm, respectively. Maximum power output was acquired to be 129.52 W, at 4 bar and 350 rpm, and maximum torque value was acquired to be 5.69 Nm, at 5 bar and 114 rpm. Moreover, it was determined that maximum power output value acquired in the titanium displacer piston at 4 bar was 3.35% more in comparison with the stainless steel displacer piston. The maximum power values acquired from the experiments conducted using the titanium displacer piston and nitrogen, air, and carbon dioxide gases as a working fluid are 129.52, 119.58, and 53.33 W, respectively. Furthermore, it was determined that maximum power output value acquired by using nitrogen gas as working fluid at 4 bar produced 7.68% and 41.2% more power, respectively, than that acquired by using air and carbon dioxide gases.

The change in the engine performance characteristics, depending on engine speed, acquired in the experimental studies conducted with stainless steel and titanium displacer pistons and air as working fluid at different engine charge pressures, is given in Figure 14. As seen in Figure 14A, the maximum power values in the experiments conducted with a stainless steel displacer piston were acquired to be 79.11, 95.67, 111.76, 124.06, and 101.42 W, respectively, for pressures of 1 to 5 bar. Maximum torque values were measured to be 3.29, 4.5, 5.46, 6.5, and 5.94 Nm, respectively. Maximum power output was acquired to be 124.04 W at 4 bar and 250 rpm, and

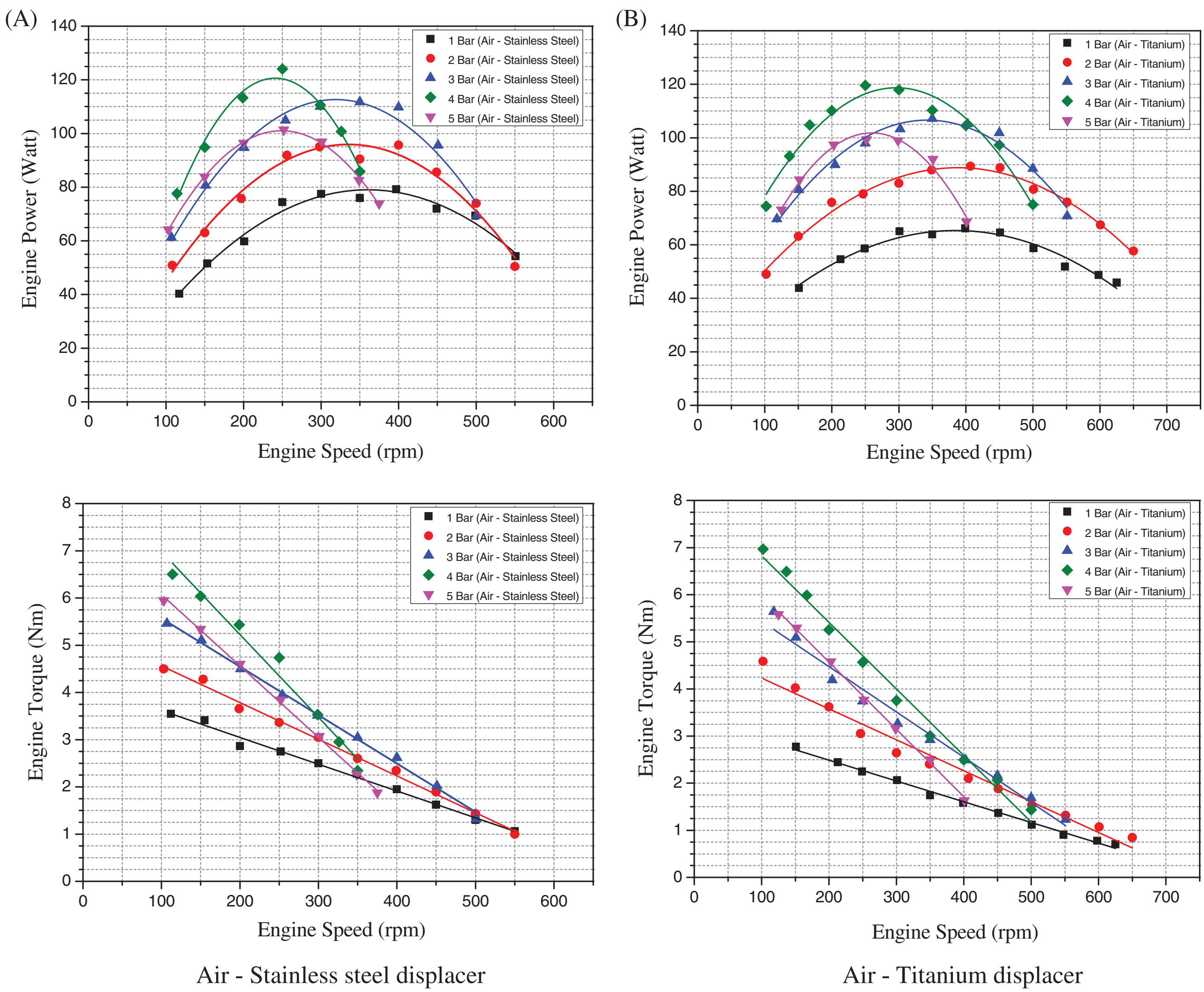

FIGURE 14 The variations of engine power and torque depending on engine speeds at different charge pressures [Colour figure can be viewed at wileyonlinelibrary.com]

maximum torque value was acquired to be 6.5 Nm at 4 bar and 114 rpm. The amount of power acquired from the engine at an engine speed of 250 to 350 rpm at all pressure values is high. This engine speed range provides the most suitable operating conditions in case of using air as the working fluid. It was determined that when a stainless steel displacer piston and air as working fluid were used, the engine speed could reach up to 550 rpm.

As seen in Figure 14B, the maximum engine power values in the experiments conducted with a titanium displacer piston were acquired to be 66.17, 89.36, 107.13, 119.58, and 99.37 W, respectively, for pressures of 1 to 5 bar. Maximum torque values were measured to be 2.77, 4.58, 5.64, 6.97, and 5.58 Nm, respectively. Maximum power output was acquired to be 119.58 W, at 4 bar and 250 rpm, and maximum torque value was acquired to be 6.97 Nm, at 4 bar and 102 rpm. The highest torque values in the engine were determined in the engine speed ranges of 100 to 150 rpm. It was revealed that when a titanium displacer piston and air as working fluid were used, the engine speed could reach up to 650 rpm. In the titanium displacer piston, it was observed that the engine power decreased, and the operating speed range of the engine was expanded compared to the stainless steel displacer piston. Furthermore, it was determined that maximum power output value acquired at 4 bar in the titanium displacer piston was 3.61% less in comparison with the stainless steel displacer piston.

The change in the engine performance characteristics, depending on engine speed, acquired in the experimental studies conducted with stainless steel and titanium material displacer pistons and carbon dioxide as working fluid at different engine charge pressures, is given in Figure 15. As seen in Figure 15A, the maximum power

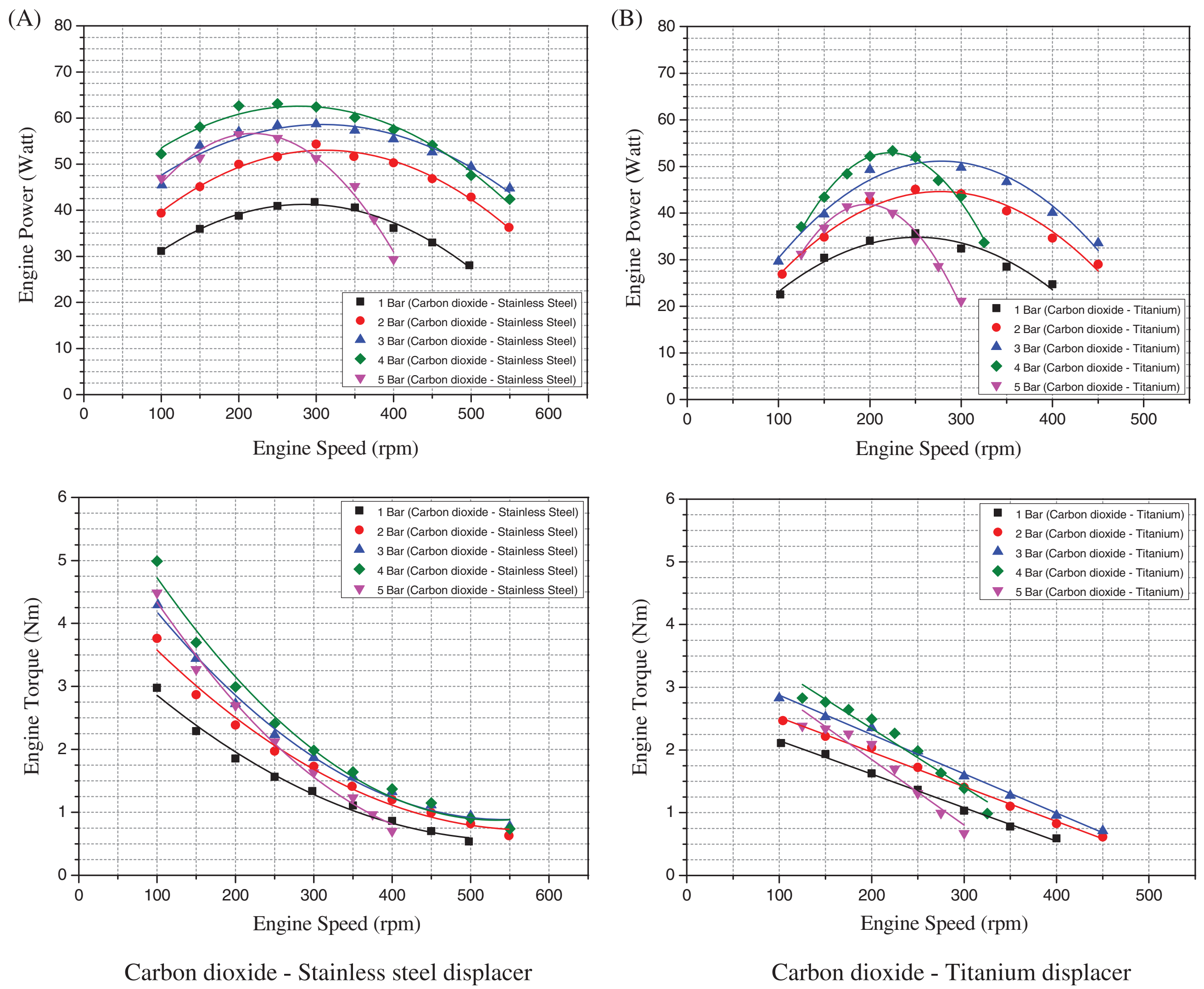

FIGURE 15 The variations of engine power and torque depending on engine speeds at different charge pressures [Colour figure can be viewed at wileyonlinelibrary.com]

values in the experiments conducted with a stainless steel displacer piston were acquired to be 41.8, 54.36, 58.7, 63.1, and 56.44 W, respectively, for pressures of 1 to 5 bar. Maximum torque values were measured to be 2.98, 3.76, 4.29, 4.98, and 4.48 Nm, respectively. In the case of using carbon dioxide gas, maximum power output was acquired to be 63.1 W, at 4 bar and 250 rpm, and maximum torque value was acquired to be 4.98 Nm, at 4 bar and 100 rpm.

As seen in Figure 15B, maximum engine power values in the experiments conducted with a titanium displacer piston were acquired to be 35.70, 45.08, 51.90, 53.33, and 43.83 W, respectively, for pressures of 1 to 5 bar. Maximum torque values were measured to be 2.11, 2,47, 2.83, 2.83, and 2.38 Nm, respectively. Maximum power output was acquired to be 53.33 W, at 4 bar and 225 rpm, and maximum torque value was acquired to be 2.83 Nm, at 4 bar and 125 rpm. Furthermore, it was determined that maximum power output value acquired at 4 bar in the titanium displacer piston was 15.48% less in comparison with the stainless steel displacer piston.

The change in the engine performance characteristics, depending on engine speed, acquired in the experimental studies conducted with stainless steel and titanium material displacer pistons and argon as working fluid at different engine charge pressures, is given in Figure 16. As seen in Figure 16A, the maximum power values in the experiments conducted with a stainless steel displacer piston were acquired to be 28.82, 41.52, 49.45, 55.42, and 49.28 W, respectively, for pressures of 1 to 5 bar. Maximum torque values were measured to be 2.1, 2.67, 3.07, 3.35, and 3.13 Nm, respectively. In the case of using argon gas, maximum power output was acquired to be 55.42 W, at 4 bar and 251 rpm, and maximum torque

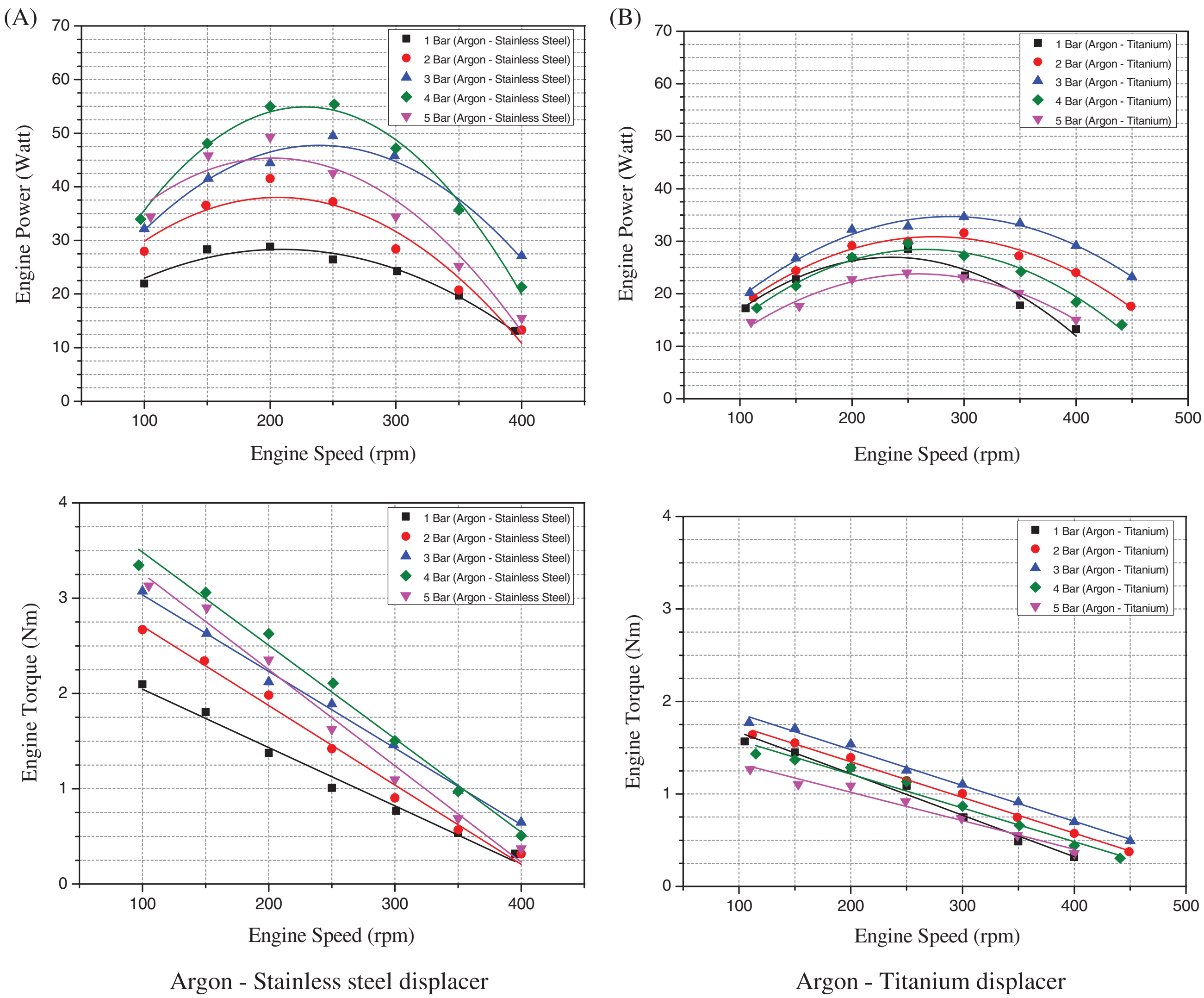

FIGURE 16 The variations of engine power and torque depending on engine speeds at different charge pressures [Colour figure can be viewed at wileyonlinelibrary.com]

value was acquired to be 3.35 Nm, at 4 bar and 97 rpm. While the thermal conductivity of argon gas at 1000 K temperature is 0.0493 W/mK, the thermal conductivity of air at the same temperature is 0.0675 W/mK. Thermal conductivity of working fluids has a very significant effect on engine performance characteristics. Therefore, thermal conductivity of working fluid determines the amount of heat energy transferred from hot source to working

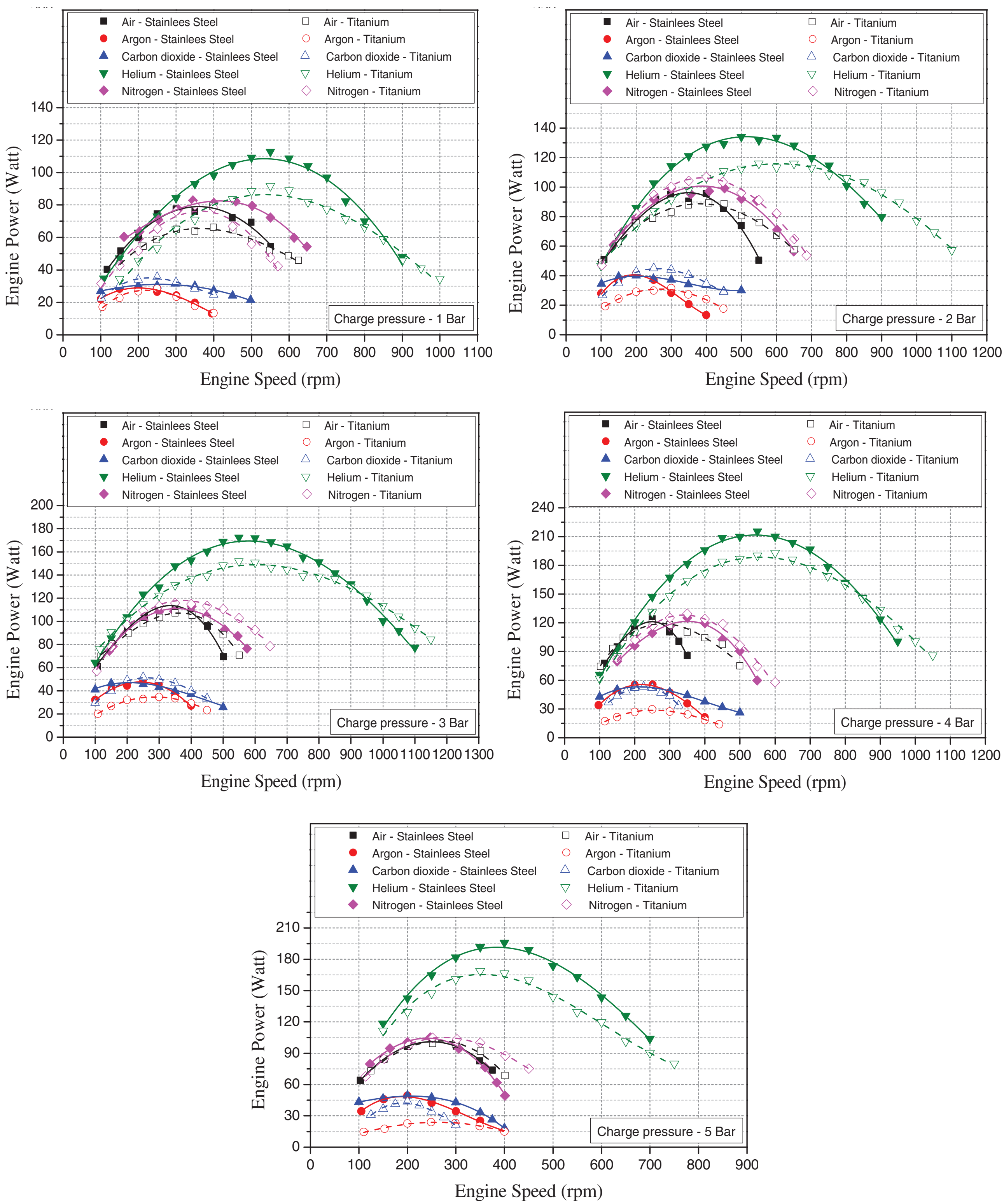

FIGURE 17 The comparison of engine powers depending on different engine speeds [Colour figure can be viewed at wileyonlinelibrary.com]

fluid, from working fluid to the cold source, and the heating and cooling times. The low thermal conductivity of the working fluid reduces the heat energy transferred to the working fluid. Therefore, engine power in using argon as working fluid is lower than gases with high thermal conductivity, and power loss is experienced. Furthermore, factors such as the high viscosity and density of argon gas compared to other gases adversely affect the engine performance.

As seen in Figure 16B, maximum engine power values in the experiments conducted with a titanium displacer piston were acquired to be 28.46, 31.59, 34.66, 29.63, and 23.99 W, respectively, for pressures of 1 to 5 bar. Maximum torque values were measured to be 1.57, 1.64, 1.77, 1.43, and 1.27 Nm, respectively. Maximum power output was acquired to be 34.66 W, at 3 bar and 300 rpm, and maximum torque value was acquired to be 1.77 Nm, at 3 bar and 109 rpm. Moreover, it was determined that maximum power output value acquired at 3 bar in the titanium displacer piston was 37.46% less than maximum power output value acquired at 4 bar in the stainless steel displacer piston.

The comparison of the maximum engine power and torque values of the stainless steel and titanium displacer pistons of different working fluids according to the engine speed is given in Figure 17. As seen in Figure 17, in the experimental studies carried out under the same conditions, the working fluids giving the highest engine output power were obtained in descending order as helium, nitrogen, air, carbon dioxide, and argon gases, respectively. It is observed that the maximum engine speeds that can be achieved in the titanium displacer piston are higher than those obtained in the stainless steel displacer piston. However, the titanium displacer piston not only increases the engine operating range but also reduces the engine power to a certain extent. The reason for this decrease in engine power is thought to originate from the decrease in heating-cooling times at high engine speeds and the insufficient heat transfer surface area. As can be understood from the graphs obtained, it is observed that the use of carbon dioxide and argon gases as a working fluid in Stirling engines is not appropriate.

The comparison of maximum engine power and torque values of stainless steel and titanium displacer pistons of different working fluids according to the charge pressure is given in Figures 18 and 19, respectively. Maximum power output in all experimental studies was acquired to be 215.48 W, at 4 bar and 550 rpm when a stainless steel displacer piston and helium gas as working fluid were used, and maximum torque value was acquired to be 7.54 Nm, at 5 bar and 150 rpm. This engine power acquired is the highest value acquired under all experimental conditions with stainless steel and titanium displacer pistons and nitrogen, air, carbon dioxide, and argon gases. The lowest engine power among the maximum engine powers was acquired to be 34.66 W when argon gas was used as working fluid at 3 bar and 300 rpm using a titanium displacer piston.

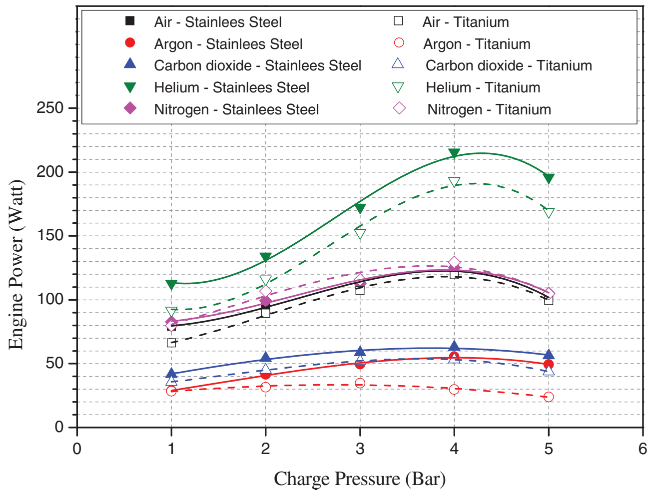

FIGURE 18 The comparison of maximum engine powers depending on charge pressure [Colour figure can be viewed at wileyonlinelibrary.com]

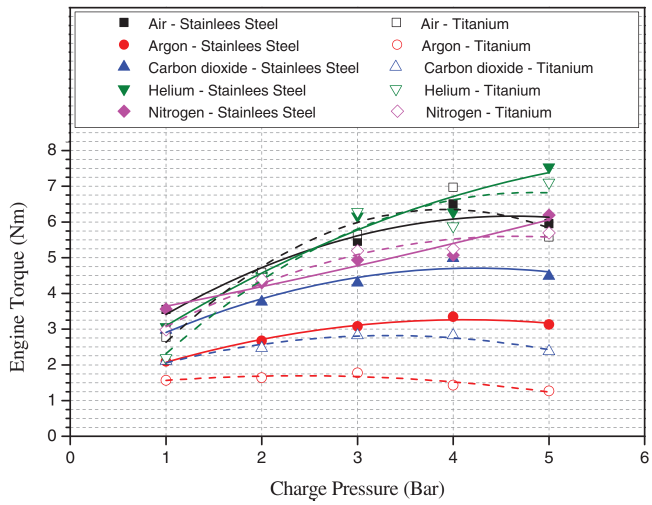

FIGURE 19 The comparison of maximum engine torques depending on charge pressure [Colour figure can be viewed at wileyonlinelibrary.com]

The lowest engine power was acquired to be 23.99 W using a titanium displacer piston at 5 bar and 249 rpm in case of using argon gas as working fluid, and the lowest engine torque value was acquired to be 1.27 Nm, at 5 bar and 110 rpm.

In the experiments conducted with a stainless steel and titanium displacer piston using helium, nitrogen, air, and carbon dioxide gases as working fluids, maximum

TABLE 2 The comparison of maximum engine powers depending on displacer piston material

	Stainless steel displacer piston			Titanium displacer piston		
Working fluid	Charge pressure (bar)	Engine speed (rpm)	Max. Power (W)	Charge pressure (bar)	Engine speed (rpm)	Max. Power (W)
Helium	4	550	215.48	4	600	193.12
Nitrogen	4	350	125.19	4	350	129.52
Air	4	250	124.06	4	250	119.58
Carbon dioxide	4	250	63.1	4	225	53.3
Argon	4	250	55.42	3	300	34.66

power output occurred at 4 bar. However, in the experiments conducted with argon gas and a titanium displacer piston, it was determined that maximum power output was generated at 3 bar.

The working fluids used in Stirling engines are applied as much as the amount of charge pressure required from the crankcase. Therefore, the charge pressure in the crankcase creates a counterforce at the bottom side of the power piston. This counterforce has an adverse effect on engine power at high charge pressures. Moreover, the amount of gas used at 1 bar charge pressure and the amount of gas used at 5 bar charge pressure are different, in the crankcase. Therefore, while the required heating and cooling times for the low-pressure working fluid are sufficient, they are not sufficient for the working fluid at high pressures. Moreover, as the engine speed increases, the heating and cooling times required for the working fluid shorten, and the engine power values decrease. Another reason for the decrease in engine power output values with the increase in charge pressure is the high friction that occurs as a result of contact of increased amount of gas in the cylinder with the cylinder walls and piston surfaces. As the engine speed increases at high pressures, friction, heat leakage, and mechanical losses become more effective. These losses reduce the engine power output.

As can be seen in Table 2, the maximum power values acquired from different working fluids differ according to the charge pressure, engine speed, and the material type of the displacer piston. In all working fluids except for nitrogen, the stainless steel displacer piston performed better than titanium displacer piston. Among all the experimental studies, the most efficient performance values were acquired when the stainless steel displacer piston and helium gas were used.

Maximum power output acquired in experimental studies with a stainless steel displacer piston and helium was determined to be 72.12%, 73.69%, 241.49%, and 288.81% higher than the power acquired by nitrogen, air, carbon dioxide, and argon gases, respectively.

5 | CONCLUSIONS

In this study, a Stirling engine with rhombic mechanism which has a swept volume of 365 cm^3 was designed, manufactured and tested. The performance tests of engine with a rhombic mechanism were conducted under the laboratory conditions using an electric heater as a heat source at 1000 K heater temperature and using helium, nitrogen, air, carbon dioxide, and argon as working fluid at different charge pressures. A prony-type dynamometer was developed and the Stirling engine's power and torque values were determined as experimentally. The effects of basic parameters related to engine performance such as working fluid mass, charge pressure and heater temperatures on net work amount were also investigated. As a result of theoretical and experimental studies, the following evaluations can be made for the Stirling engine with a rhombic mechanism.

- During thermodynamic analyses mass of working fluid was kept constant at 0.000536 kg and the coolant temperature was kept constant at 300 K. The cyclic work values of this engine with a rhombic mechanism were calculated as 10.66, 11.61, and 12.42 J at 900, 1000, and 1100 K heater temperatures, respectively.
- The heater and coolant temperatures were kept constant at 1000 K and 300 K, respectively, during a cycle for 1, 2, 3, 4, and 5 bar charge pressures. Under these conditions, the cyclic work values of this engine with a rhombic mechanism were acquired as 11.61, 23.22, 34.83, 46.44, and 58.05 J, respectively.
- In all experimental studies, maximum power output was acquired to be 215.48 W at 4 bar charge pressure and an engine speed of 550 rpm when a stainless steel displacer piston and helium gas as working fluid were used, and maximum torque value was acquired to be 7.54 Nm, at 5 bar charge pressure and an engine speed of 150 rpm.
- The lowest engine power output among the maximum engine powers was acquired to be 34.66 W, when

argon gas was used as working fluid at 3 bar charge pressure and 300 rpm, using a displacer piston made of titanium material.

- Among all experimental studies, the lowest engine power was acquired to be 23.99 W when argon gas was used as working fluid at 5 bar charge pressure and 249 rpm, using a displacer piston made of titanium material, and the lowest engine torque value was acquired to be 1.27 Nm, at 5 bar charge pressure and 110 rpm.
- In the experiments conducted with stainless steel and titanium displacer pistons and using helium, nitrogen, air, and carbon dioxide gases as working fluids, maximum power output occurred at 4 bar charge pressure. However, in the experiments conducted with argon gas and displacer piston made of titanium material, it was determined that maximum power output occurred at 3 bar charge pressure.
- The most efficient performance values among all the experimental studies conducted were acquired when displacer piston made of stainless steel and helium as a working fluid was used.
- Due to the lower thermal conductivity, higher viscosity, and higher density of argon compared to other working fluids, its engine performance acquired in both stainless steel and titanium displacer pistons was the lowest in comparison with other gases.

ACKNOWLEDGEMENT

This study was supported within the scope of the projects numbered MUH19002.18.001 and MUH19004.19.001 by Hitit University, Department of Scientific Research Projects. We would like to thank Hitit University, Department of Scientific Research Projects for its financial support.

NOMENCLATURE

A_d	displacer piston area (m^2)
A_{dr}	displacer rod area (m^2)
A_p	power piston area (m^2)
Dd	displacer cylinder bore (mm)
Dp	power cylinder bore (mm)
Dr	displacer rod bore (mm)
e_c	length of compression space (mm)
e_e	length of expansion space (mm)
hd	displacer piston length (mm)
hp	power piston length (mm)
Ht	cylinder length (mm)
J	joule
L	distance between gear axes (mm)
ldr	displacer rod length (mm)
lr	connecting rod length of rhombic (mm)
m	mass of working fluid
n	engine speed (rpm)
Nm	newton meter
P	pressure (kPa)
R	gas constant (kJ/kgK)
Rc	crank radius (mm)
T	temperature (K)
T_H	heater temperature (K)
T_L	cooler temperature (K)
rpm	revolutions per minute
V	volume
V_c	volume of compression space
V_e	volume of expansion space
W	engine output work
W	watt
Y_d	the distance from top point of displacer piston to the axis of the crank
Y_p	the distance from top point of power piston to the axis of the crank

DATA AVAILABILITY STATEMENT

All data can be provided explicitly.

ORCID

Derviş Erol https://orcid.org/0000-0002-3438-9312
Sinan Çalışkan https://orcid.org/0000-0002-7753-0355

REFERENCES

1. Barreto RA. Fossil fuels, alternative energy and economic growth. *Econ Model*. 2018;75:196-220.
2. Mohr SH, Wang J, Ellem G, Ward J, Giurco D. Projection of world fossil fuels by country. *Fuel*. 2015;141:120-135.
3. Sathre R. Comparing the heat of combustion of fossil fuels to the heat accumulated by their lifecycle greenhouse gases. *Fuel*. 2014;115:674-677.
4. Gielen D, Boshell F, Saygin D, Bazilian MD, Wagner N, Gorini R. The role of renewable energy in the global energy transformation. *Energ Strat Rev*. 2019;24:38-50.
5. Hansen K, Mathiesen BV, Skov IR. Full energy system transition towards 100% renewable energy in Germany in 2050. *Renew Sust Energ Rev*. 2019;102:1-13.
6. Krakowski V, Assoumou E, Mazauric V, Maïzi N. Reprint of feasible path toward 40–100% renewable energy shares for power supply in France by 2050: a prospective analysis. *Appl Energy*. 2016;184:1529-1550.
7. Bulut U, Muratoğlu G. Renewable energy in Turkey: great potential, low but increasing utilization, and an empirical analysis on renewable energy-growth nexus. *Energy Policy*. 2018; 123:240-250.
8. Finkelstein T, Organ AJ. *Air Engines the History Science and Reality of the Perfect Engine*. New York: The American Society of Mechanical Engineers; 2004.
9. Rinia H, Pre FKD. Air engines. *Philips Techn Rev*. 1946;8: 129-136.
10. Meijer RJ. Philips Stirling engine activities. SAE Technical Paper, No. 650004, 1965.

11. Erol D, Yaman H, Doğan B. A review development of rhombic drive mechanism used in the Stirling engines. *Renew Sust Energ Rev*. 2017;78:1044-1067.
12. Hargreaves CM. *The Philips Stirling Engine*. New York: Elsevier; 1991.
13. White MA, Qiu S, Olan RW, Erbeznik RM. Technology demonstration of a free-piston Stirling advanced radioisotope space power system. *AIP Conference Proceedings, American Institute of Physics*. 1999;458(1):1413-1419.
14. Solomon L, Qiu S. Computational analysis of external heat transfer for a tubular Stirling convertor. *Appl Therm Eng*. 2018; 137:134-141.
15. Qiu S, Gao Y, Rinker G, Yanaga K. Development of an advanced free-piston Stirling engine for micro combined heating and power application. *Appl Energy*. 2019;35:987-1000.
16. Zare S, Tavakolpour-Saleh A. Free piston Stirling engines: a review. *Int J Energy Res*. 2020;44(7):5039-5070.
17. Shufat SA, Kurt E, Cinar C, Aksoy F, Hançerlioğulları A, Solmaz H. Exploration of a Stirling engine and generator combination for air and helium media. *Appl Therm Eng*. 2019;150: 738-749.
18. Ahmed F, Huang H, Ahmed S, Wang X. A comprehensive review on modeling and performance optimization of Stirling engine. *Int J Energy Res*. 2020;44(8):6098-6127.
19. Lienesch JH, Wade WR. Stirling engine progress report: smoke, odor, noise and exhaust emissions. SAE Technical Paper, No. 680081, 1968.
20. Eid E. Performance of a beta configuration heat engine having a regenerative displacer. *Renew Sust Energ Rev*. 2009;34:2404-2413.
21. Shendage DJ, Kedare SB, Bapat SL. An analysis of beta type Stirling engine with rhombic drive mechanism. *Renew Energy*. 2011;36:289-297.
22. Solmaz H, Karabulut H. Performance comparison of a novel configuration of beta type Stirling engines with rhombic drive engine. *Energy Convers Manag*. 2014;78:627-633.
23. Aksoy F, Solmaz H, Karabulut H, Çınar C, Özgören YÖ, Polat S. A thermodynamic approach to compare the performance of rhombic drive and crank drive mechanisms for a beta type Stirling engine. *Appl Therm Eng*. 2016;93:359-367.
24. Salazar JL, Chen W-L. A computational fluid dynamics study on the heat transfer characteristics of the working cycle of a beta type Stirling engine. *Energy Convers Manag*. 2014;88: 177-188.
25. Chen W-L, Wong K-L, Chang Y-F. A numerical study on the effects of moving regenerator to the performance of a beta type Stirling engine. *Int J Heat Mass Transf*. 2015;83:499-508.
26. Zainudin MF, Abu Bakar R, Ming GL, Ali T, Sup BA. Thermodynamic cycle evaluation of rhombic drive beta configuration Stirling engine. *Energy Procedia*. 2015;68:419-428.
27. Xiao G, Chen C, Shi B, Cen K, Ni M. Experimental study on heat transfer of oscillating flow of a tubular Stirling engine heater. *Int J Heat Mass Transf*. 2014;71:1-7.
28. Ni M, Shi B, Xiao G, Luo Z, Cen K. Heat transfer characteristics of the oscillating flows of different working gases in U-shaped tubes of a Stirling engine. *Appl Therm Eng*. 2015;89:569-577.
29. Luo Z, Sultan U, Ni M, Peng H, Shi B, Xiao G. Multi objective optimization for GPU3 Stirling engine by combining multi objective algorithms. *Renew Energy*. 2016;94:114-125.
30. Ni M, Shi B, Xiao G, et al. Improved simple analytical model and experimental study of a 100 W beta type Stirling engine. *Appl Energy*. 2016;169:768-787.
31. Xiao G, Sultan U, Ni M, et al. Design optimization with computational fluid dynamic analysis of beta type Stirling engine. *Appl Therm Eng*. 2017;113:87-102.
32. Wang K, Dubey S, Choo FH, Duan F. A transient one dimensional numerical model for kinetic Stirling engine. *Appl Energy*. 2016;183:775-790.
33. Abuelyamen A, Ben-Mansour R, Abualhamayel H, Mokheimer EMA. Parametric study on beta type Stirling engine. *Energy Convers Manag*. 2017;145:53-63.
34. Alfarawi S. Thermodynamic analysis of rhombic-driven and crank-driven beta-type Stirling engines. *Int J Energy Res*. 2020; 44(7):5596-5608.
35. Solmaz H, Ardebili SMS, Aksoy F, Calam A, Yılmaz E, Arslan M. Optimization of the operating conditions of a beta-type rhombic drive Stirling engine by using response surface method. *Energy*. 2020;198:117377.
36. Cheng CH, Yu YJ. Numerical model for predicting thermodynamic cycle and thermal efficiency of a beta type Stirling engine with rhombic drive mechanism. *Renew Energy*. 2010;35: 2590-2601.
37. Cheng CH, Yang HS. Optimization of geometrical parameters for Stirling engines based on theoretical analysis. *Appl Energy*. 2012;92:395-405.
38. Cheng CH, Yu YJ. Combining dynamic and thermodynamic models for dynamic simulation of a beta type Stirling engine with rhombic drive mechanism. *Renew Energy*. 2012;37: 161-173.
39. Cheng CH, Yang HS, Keong L. Theoretical and experimental study of a 300 W beta type Stirling engine. *Energy*. 2013;59: 590-599.
40. Cheng CH, Yang HS. Optimization of rhombic drive mechanism used in beta type Stirling engine based on dimensionless analysis. *Energy*. 2014;64:970-978.
41. Cheng CH, Chen YF. Numerical simulation of thermal and flow fields inside a 1 kW beta type Stirling engine. *Appl Therm Eng*. 2017;121:554-561.
42. Yang HS, Cheng CH, Huang ST. A complete model for dynamic simulation of a 1-kW class beta-type Stirling engine with rhombic-drive mechanism. *Energy*. 2018;161:892-906.
43. Cheng CH, Yang HS, Chen HX. Development of a beta-type Stirling heat pump with rhombic drive mechanism by a modified non-ideal adiabatic model. *Int J Energy Res*. 2020;44(7): 5197-5208.
44. Cheng C-H, Phung D-T. Numerical and experimental study of a compact 100-W-class β-type Stirling engine. *Int J Energy Res*. 2021;45:6784-6799. https://doi.org/10.1002/er.6271.
45. Li T, Tang DW, Li ZG, Du JL, Zhou T, Jia Y. Development and test of a Stirling engine driven by waste gases for the micro CHP system. *Appl Therm Eng*. 2012;33–34:119-123.
46. Duan C, Sun C, Shu S, Ding G, Jing C, Chang J. Similarity design and experimental investigation of a beta-type Stirling engine with a rhombic drive mechanism. *Int J Energy Res*. 2015;39(2):191-201.
47. Aksoy F, Çınar C. Thermodynamic analysis of a beta-type Stirling engine with rhombic drive mechanism. *Energy Convers Manag*. 2013;75:319-324.

48. Çınar C, Aksoy F, Okur M. Design, manufacturing and performance tests of a Stirling engine with rhombic drive mechanism. *J Fac Eng Archit Gazi Univ*. 2013;28:795-801.
49. Akyel E. Design and Performance Analysis of a Stirling Engine with Rhombic Drive Mechanism [master's thesis]. Afyon: Afyon Kocatepe University, Institute of Science and Technology; 2015.
50. Arslan M. The Performance Tests of a Beta Type Rhombic Drive Stirling Engine with Regenerator [master's thesis]. Afyon: Afyon Kocatepe University, Institute of Science and Technology; 2016.
51. Aksoy F, Solmaz H, Çınar C, Karabulut H. 1.2 kW beta type Stirling engine with rhombic drive mechanism. *Int J Energy Res*. 2017;41:1310-1321.
52. Çınar C, Solmaz H, Ipci D, Yılmaz E, Aksoy F. Performance enhancement of a beta type rhombic drive Stirling engine. *Int J Green Energy*. 2020;17(13):884-893.
53. Meijer RJ. The Philips hot gas engine with rhombic drive mechanism. *Philips Techn Rev*. 1959;20:245-276.
54. Urieli I, Berchowitz DM. *Stirling Cycle Engine Analysis*. Bristol: Adam Hilger Ltd; 1984.
55. Schmidt G. Theorie der Lehmann'schen Calorischen Maschine (theory of Lehmann's caloric machine). *Zeitschrift Des Vereins Deutscher Ingenieure*. 1871;15:98-112.
56. Bolzoni L, Ruiz-Navas EM, Gordo E. Flexural properties, thermal conductivity and electrical resistivity of prealloyed and master alloy addition powder metallurgy Ti-6Al-4V. *Mater Des*. 2013;52:888-895.
57. Mohr M, Wunderlich R, Novakovic R, Ricci E, Fecht HJ. Precise measurements of thermophysical properties of liquid Ti-6Al-4V (Ti64) alloy on board the international space station. *Adv Eng Mater*. 2020;22(7):2000169.

How to cite this article: Erol D, Çalışkan S. The examination of performance characteristics of a beta-type Stirling engine with a rhombic mechanism: The influence of various working fluids and displacer piston materials. *Int J Energy Res*. 2021;45:13726–13747. https://doi.org/10.1002/er.6702